



Hydrodynamic modeling of coastal seas: the role of tidal dynamics in the Messina Strait, Western Mediterranean Sea

A. Cucco*, G. Quattrocchi, A. Olita, L. Fazioli, A. Ribotti, M. Sinerchia, C. Tedesco and R. Sorgente

5 National Research Council, Institute for Coastal Marine Environment, Oristano, 09170 Italy

*Correspondence to: A. Cucco (andrea.cucco@cnr.it)

Abstract. This work explored the importance of considering tidal dynamics when modeling the general circulation in the Messina Strait, a narrow passage connecting the Tyrrhenian and the Ionian Sea sub-basins in the Western Mediterranean Sea. The tides and the induced water circulation in this Strait are among the most intense oceanographic processes in the
10 Mediterranean Sea. The quantification of these effects can be particularly relevant for operational oceanographic systems aimed to provide short-term predictions of the main hydrodynamics in the Western Mediterranean sub-basins. A numerical approach based on the use of a high resolution hydrodynamic model was adopted to firstly reproduce both the tides propagation and the wind induced and thermohaline water circulation within the Strait and surrounding areas and secondly to quantify the role of the Strait dynamics on the outer water circulation. The obtained results confirmed the importance of a
15 correct representation of the hydrodynamics in the Messina Strait even when focusing on predicting the water circulation in the external sea traits. In fact, model results show that tidal dynamics deeply impact the reproduction of the instantaneous and residual circulation pattern, waters thermohaline properties and transport dynamics both inside the Messina Strait and in the surrounding coastal and open waters.

1 Introduction

20 In the XII chapter of the Odyssey, before the landing to Trinacria Island, Ulysses and his crew leaving the Circe refuge, experienced the wrath of Scilla and Cariddi, with great loss of men and ships (Homer, VI B.C.). The Homer's poem, describing the intense vortices and heavy currents generated by the tides (Scilla and Cariddi) in the Messina Strait (Western Mediterranean Sea, hereafter MS), can be considered one of the first examples of grey literature in physical Oceanography. The tides and the induced water circulation in this Strait (figure 1a and figure 1b) are among the most interesting
25 oceanographic processes in the Mediterranean Sea, and not only because of Homer's epic. The intense current speeds and the high variability of tidal phases and frequencies lead to consider this area as one of the most energetic in terms of momentum and impulse all over the basin (Hopkins et al., 1984). This is why, in recent years,



several research activities were carried out to investigate how tidal dynamics in this area can be exploited to produce renewable energy (Coiro et al., 2013).

Even if notorious, the dynamic of the Strait is not fully addressed in scientific literatures, with only few and old studies describing the water circulation in both theoretical and experimental terms (Hopkins et al., 1984; Cescon et al., 1997) and
5 very few recent investigations using numerical modelling techniques (Androsov et al., 2002a; Androsov et al., 2002b). In particular, while tidal dynamic inside the Strait has been studied and described by many authors starting from the early XX century (Vercelli, 1925; Vercelli, 1926; Defant, 1940; Bossolasco and Dagnino, 1957; Defant, 1961; Massi and Sallusti, 1979; Mosetti 1988), the effects of the Messina tidal in and outflow on the outer open ocean thermohaline water circulation is still unaddressed in scientific literature. In particular, both recent and old studies focused mainly on describing the
10 behaviour of Tyrrhenian and Ionian waters flowing through the Strait (Bossolasco and Dagnino, 1959; Androsov et al., 2002b) and on the generation of internal waves (Brandt et al., 1997; Brandt and Rubino, 1999) without quantifying the role of MS tidal dynamics in modifying the outer circulation pattern.

The quantification of these effects can be particularly relevant for operational oceanographic systems aimed to provide short term predictions of the main hydrodynamics in the Western Mediterranean sub-basins. Most of this ocean prediction systems
15 (Tonani et al., 2008; Oddo et al., 2009; Pinardi et al., 2010; Sorgente et al., 2011; Tonani et al., 2015) are not suitable to accurately reproduce the Strait dynamics mainly due to numerical grid limitation, where orthogonality and spatial resolution are not appropriate to describe fine scale coastal features. As a consequence, the operational output of such systems provide temperature, salinity and water currents fields, which are estimated ignoring the contribution of tidal exchanges within the Strait capable of modifying the water current, salinity and temperature fields as well as the water mass budgets between the
20 sub-basins.

Consequently, the question is: how big is the effect accurately capturing finer scale processes, such as tidal dynamics, on the model reproduction of the circulation in the area? This issue is particularly relevant in the case of MS, that is characterized by intense tidal dynamics, quite a unique case in the Mediterranean sea, where tides are generally weak and have a low influence on circulation (Sannino et al., 2015).

25 In this work, a numerical approach based on the use of a high resolution hydrodynamic model based on finite elements method was proposed to reproduce both the tides propagation and the wind induced and thermohaline circulation in the Strait and surrounding areas and to quantify the role of the Strait dynamics on the outer water circulation. Three different scenarios characterized by different model forcings were investigated in order to identify the weight of each single contribution (tides, thermohaline and wind) to the main hydrodynamics in the area of interest.

30 The paper is organized as follows: a brief description of the MS study area, including the morphological and oceanographic features is reported in Section 2. An overview of the applied method including the description of the adopted numerical model and of the three simulated scenarios is reported in Section 3. In Section 4, the differences between the three scenarios results are analysed highlighting the importance of reproducing the tidal dynamics in the MS. Finally in Section 5, the conclusive remarks.



2 The study site

The Messina Strait (figures 1a and 1b) is a narrow and deep channel connecting two Mediterranean sub-basins: the Tyrrhenian and the Ionian Sea. The channel is 70 km long and 10 km wide with the narrowest passage of about 3 km width. The main axis is north-south oriented slightly bending eastward in correspondence of the northern opening. The water depth at the mouths of the strait varies between 500 m and 600 m, abruptly decreasing to 100 m in correspondence of a sill in the narrowest passage.

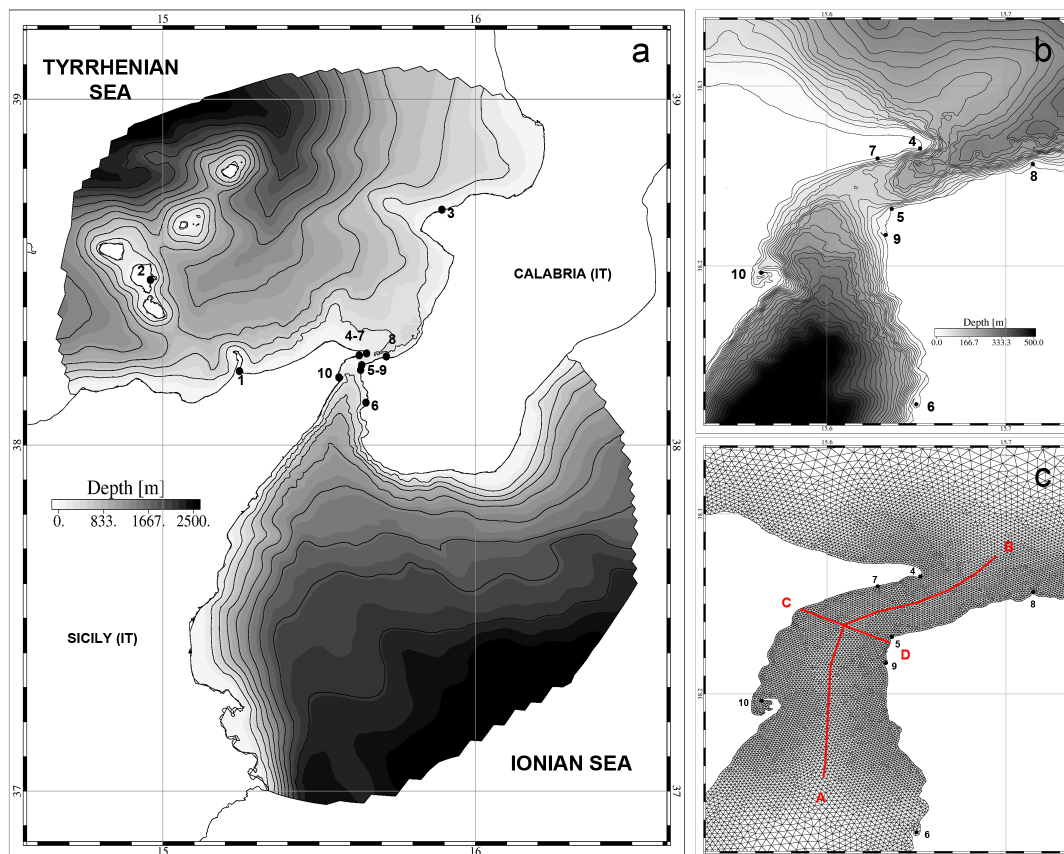


Figure 1: Geographical settings and model domain: investigated area comprising the Messina Strait the southern Tyrrhenian Sea and part of Ionian Sea, geometry and bathymetry (panel a). Black dots and numbers indicate the tide gauge locations at Milazzo (1), Lipari (2) Tropea (3), Faro (4), Villa S. Giovanni (5) Reggio (6), Messina (7), Ganzirri (8), Punta



Pezzo (9) and Messina (10); zoom of the Messina Strait (panel b); zoom of the finite element mesh adopted for numerical simulations (panel b). Red lines from A to B and from C to D indicate the sections used for the flux computation and model results analysis.

5 The astronomic tides represent the main forcing driving the water circulation inside the channel, which occurs mainly along the major axis. The water vertical displacement varies between 0.2 and 0.3 m, which are the typical values for tidal amplitudes in the Western Mediterranean Sea. Despite the very low amplitudes, the water flow inside the Strait is very intense reaching up to 2.5 m/s during the spring tides. The frequency is mainly semidiurnal, with the M2 and S2 being the most intense constituents, but also with a strong contribution by the overtides, M4, which are generated by the nonlinear
10 interaction between the semidiurnal constituents and between the tidal waves and the complex Strait topography (Carta et al., 2008).

The flow inside the Strait is directed northward during the flood phase and southward during the ebb phase. The interaction between the intense currents and the channel topography and bathymetry gives rise to the formation of inertial eddies and strong horizontal current shears generally located at the lee-sides of both Sicily and Calabria main capes.

15 The Strait connects two sub-basins with different oceanographic features. The northern part of the Strait opens on the Southern Tyrrhenian Sea which is characterized by the presence of a west to east flow located between 50 and 200 m, carrying the surface Atlantic Water (AW) toward the northern part of the sub-basin moving geostrophically along the Italian coast (Krivosheya, 1983; Astraldi and Gasparini, 1994; Millot, 1999; Vetrano et al., 2004). The Southern part of the Strait opens on the Western Ionian Sea characterized by a surface flow carrying the Ionian waters from the southern Calabria
20 coastlines along the eastern side of Sicily coastlines southward to the Sicily channel.

3 The method

The tidal dynamics and water exchange in the Messina Strait and their influence on the general water circulation in the Southern Tyrrhenian and Ionian Sea are investigated following a numerical approach.

A high resolution hydrodynamic model (SHYFEM, hereafter, Umgiesser et al., 2004), based on the finite element method
25 applied to Messina Strait, Southern Tyrrhenian Sea and part of the Ionian Sea was adopted to reproduce the main hydrodynamic inside the Strait and in the surrounding open sea areas. This model is part of the operational system MeSOS (Messina Strait Operational System), developed under the framework of TESSA (Technologies for the Situational Sea Awareness) project funded by the Italian Ministry for Environment, aiming to develop an innovative operational platform for the sea awareness in the Mediterranean Sea.

30 SHYFEM was nested into a lower resolution open ocean model, the Tyrrhenian Sicily Channel sub-Regional Model (TSCRM, hereafter) applied to the whole Tyrrhenian Sea and Sicily Channel in order to properly account for the lateral open boundary conditions.



The TSCRM sub-regional ocean model covers the area from 8.98 E to 16.5 E in longitude and from 31 N to 43 N in latitude with a full three-dimensional implementation of the Princeton Ocean Model (Blumberg and Mellor, 1987; Mellor, 1991) and represents the updated version of the previous operational analysis/forecast model, named Sicily Channel sub-Regional Model (SCRM), operational since 2004 (Fazioli et al., 2016). The model uses an uniform horizontal orthogonal grid with a resolution of $1/48^\circ$ (2 km) in longitude and latitude (362 x 578 mesh points, respectively). The vertical direction is discretized by 30 sigma levels, which are spaced using a logarithmic distribution near the surface and uniformly in the rest of the water column. Surface boundary conditions are provided by ECMWF meteorological forecasting system. TSCRM assimilates AVISO data along track Sea Level Anomalies on a daily basis through a 3D Variational procedure (see OCEANVAR in Dobricic et al. 2008), with the same implementation described in Olita et al. (2012) for the previous version of the TSCRM operational system (SCRM, Gabersek et al. 2007). The system predicts, on hourly frequency, water currents, temperature and salinity at different water depths and for a 5 days time lag.

The nesting between SHYFEM and TSCRM was carried out following the procedure in Cucco et al., (2012) allowing to reproduce with high details both the outer general circulation and the coastal hydrodynamics (Canu et al., 2015; Marras et al., 2015).

The following section provides a description of SHYFEM, the numerical core of the system, its application to the MS, the adopted setup and the three numerical experiments performed to achieve the proposed objectives.

3.1 The hydrodynamic model

SHYFEM is a 3D hydrodynamic model based on the finite element method that resolves the shallow water equations integrated over each layer in their formulations with water levels and transports. The model has been applied with success in several applications and case studies in the Mediterranean Sea basin aimed to investigate and predict both open ocean and coastal hydrodynamics and to evaluate their mutual interactions (Bellafiore et al., 2008; Bellafiore et al., 2011; Ferrarin et al., 2013; Simeone et al., 2014; Umgiesser et al., 2014; Ferrarin et al., 2014; Quattrocchi et al., 2016).

It uses finite elements for horizontal spatial discretizations, z-layers for vertical discretizations and a semi-implicit algorithm for integration in time. The horizontal diffusion, the baroclinic pressure gradients and the advective terms in the momentum equation are fully explicit. The Coriolis force and the barotropic pressure gradients terms in the momentum equation and the divergence term in the continuity equation are semi-implicitly treated, while the vertical stress and friction terms are fully implicit for stability reasons. The model is unconditionally stable for fast gravity waves, bottom friction and Coriolis acceleration. The solved equation system reads as:



$$\begin{aligned} \frac{\partial U_l}{\partial t} + Adv_l^x - fV_l = gh_l \frac{\partial \zeta}{\partial x} - \frac{gh_l}{\rho_0} \frac{\partial}{\partial x} \int_{-H_l}^{\zeta} \rho' dz + \frac{h_l}{\rho_0} \frac{\partial p_a}{\partial x} + \frac{1}{\rho_0} (\tau_x^{top(l)} - \tau_x^{bottom(l)}) + A_H \left(\frac{\partial^2 U_l}{\partial x^2} + \frac{\partial^2 U_l}{\partial y^2} \right) \\ + S_l^x + \frac{\partial}{\partial z} \left(\frac{K_l}{h_l} \frac{\partial U_l}{\partial z} \right) + gh_l \frac{\partial \eta}{\partial x} - gh_l \beta \frac{\partial \zeta}{\partial x} \end{aligned}$$

$$\begin{aligned} \frac{\partial V_l}{\partial t} + Adv_l^y + fU_l = gh_l \frac{\partial \zeta}{\partial y} - \frac{gh_l}{\rho_0} \frac{\partial}{\partial y} \int_{-H_l}^{\zeta} \rho' dz + \frac{h_l}{\rho_0} \frac{\partial p_a}{\partial y} + \frac{1}{\rho_0} (\tau_y^{top(l)} - \tau_y^{bottom(l)}) + A_H \left(\frac{\partial^2 V_l}{\partial x^2} + \frac{\partial^2 V_l}{\partial y^2} \right) \\ + S_l^y + \frac{\partial}{\partial z} \left(\frac{K_l}{h_l} \frac{\partial V_l}{\partial z} \right) + gh_l \frac{\partial \eta}{\partial y} - gh_l \beta \frac{\partial \zeta}{\partial y} \end{aligned}$$

eq. 1

$$\frac{\partial \zeta}{\partial t} + \sum_{\mathcal{T}} \frac{\partial U_l}{\partial x} + \sum_{\mathcal{T}} \frac{\partial V_l}{\partial y} = 0$$

where l indicates the vertical layer, (U_l, V_l) the horizontal transport components in x and y directions for each layer, Adv^x and Adv^y the advective terms, f the Coriolis parameter, p_a the atmospheric pressure, g the gravitational constant, ζ the water level, ρ_0 the standard water density, $\rho = \rho_0 + \rho'$ the water density, h_l the layer thickness, H_l the depth of the bottom of the layer l ,

- 5 A_H the horizontal eddy viscosity estimated following the Smagorinsky parameterization (Smagorinsky, 1963; Blumberg and Mellor, 1987).

The GOTM (General Ocean Turbulence Model) turbulence closure model described in Burchard and Petersen (1999) was used for the computation of the vertical viscosity K_l . Equilibrium tidal potential (η) and load tides are included as model forcing. The term η is computed as the sum of the tidal potential of each tidal constituents multiplied by the frequency-
 10 dependent elasticity factor (Kantha and Clayson 2000), whereas the factor β accounts for the effects of load tides (Kantha, 1995). Wind and bottom friction terms, corresponding to the boundary conditions of the stress terms (τ_x, τ_y) , are defined as:

$$\begin{aligned} \tau_x^{surface} &= C_D \rho_a w_x \sqrt{w_x^2 + w_y^2} \\ \tau_x^{bottom} &= C_B \rho_0 u_L \sqrt{u_L^2 + v_L^2} \\ \tau_y^{surface} &= C_D \rho_a w_y \sqrt{w_x^2 + w_y^2} \\ \tau_y^{bottom} &= C_B \rho_0 v_L \sqrt{u_L^2 + v_L^2} \end{aligned}$$

eq. 2

With C_D as the wind drag coefficient, C_B the bottom friction coefficient, ρ_a the air density (w_x, w_y) the wind velocity components and (u_L, v_L) the bottom velocity components.

- 15 The hydrodynamic model is coupled with advection and diffusion numerical module which takes into account salt and thermal balance equations to simulate the transport of both passive tracers and salinity and temperature in the domain. Details of numerical treatments are reported in Umgiesser et al., (2004).



3.2 Model and simulation setup

SHYFEM uses finite elements unstructured mesh for representing the model domain. A grid composed of about 23000 nodes and 45000 triangular elements was implemented. The mesh reproduces the MS, the South Eastern Tyrrhenian Sea and part of the Western Ionian Sea. In Figure 1a the model domain extension is represented by the area with bathymetric details. The elements size and shape distribution is modulated accounting for both the distance from the MS and the basin morphological features. In particular, the spatial resolution varies between 50 m inside the MS and 2 km in the outer areas, corresponding to the mesh size of the TSCRM open ocean model (figure 1c).

Two open boundaries were defined in correspondence of the northern and southern mesh borders located in the inner Tyrrhenian Sea and in the Ionian Sea respectively (figure 1a). The model domain was vertically discretized with 30 levels ranging between 5 and 800 meters. At the closed boundaries, only the normal velocity is set to zero, whereas the tangential velocity is a free parameter corresponding to a full slip conditions. The same model parameters setup defined in Ferrarin et al., (2013) was adopted.

Three different simulations, with three different setups defining three different scenarios, were carried out. In the first scenario (Tide Only, TDO, hereafter), SHYFEM was used to reproduce the tidal propagation in the MS and surrounding areas.

In the second scenario (atmospheric and ThermoHaline forcing Only, THO, hereafter), the model was used to reproduce the wind induced and thermohaline circulation in the area by downscaling the sub-regional model (TSCRM) solutions to the high resolution model (SHYFEM) domain.

In the third scenario (Tide, Thermohaline and atmospheric Contributions, TTC, hereafter), SHYFEM was used to reproduce the general circulation in the area induced by both thermohaline and wind forcing and by astronomic tides. For all scenarios, simulations referred to the period between 01/01/2014 and 31/12/2015.

In table 1, the summary of the forcing data adopted for the three scenarios is provided. Open boundary conditions for TDO scenario consisted in a set of 2 years time series of hourly water levels data extracted from a regional tidal model of the Mediterranean and Black Sea (<http://volkov.oce.orst.edu/tides/otps.html>)

For THO scenario, the open boundary conditions consisted in a set of hourly time series of water levels, temperature (T) and salinity (S), computed by TSCRM for the considered period for each SHYFEM boundaries node and at each vertical level. Meteorological forcing including wind, precipitation, thermal fluxes reanalysed data, were provided at 6 hours frequency by ECMWF forecasting system.

Similarly, for the TTC scenario, the same ocean and meteorological data were used as open boundary conditions with the exception of the water levels which, in this case, were derived for each point of the mesh by a linear combination between the tidal elevations time series (estimated for the TDO scenario) and the sea surface elevations computed by TSCRM (computed for THO scenario).



	SCENARIOS SETUP & FORCING		
	TDO	THO	TTC
OBC	Astronomic tides	Ocean data (T, S, u, v, eta) from TSCRM	Ocean data (T, S, u, v, eta) from TSCRM and astronomic tides
SBC	-	Wind data, heat fluxes from ECMWF	Wind data, heat fluxes from ECMWF

Table 1: SHYFEM forcing data, including open boundary conditions (OBC) and surface boundary conditions (SBC) adopted in the three numerical experiments TDO, THO and TTC.

4 Results and discussions

5 The model was applied to simulate the 3D water circulation and the T and S variability inside the MS and in the surrounding sea areas under the three described meteo-marine scenarios: TDO, THO and TTC. The obtained results were analyzed to quantify the influence of the different forcings on the hydrodynamics of the Strait and outer sea areas.

In the following, in the first part, the tidal dynamic inside the MS, as reproduced by the TDO scenario, was described in terms of water currents, fluxes and residual circulation. Subsequently, the role of the tides in modulating the wind induced and thermohaline circulation was investigated both inside and outside the MS by comparing the THO and TTC scenarios results. Residual circulation, water fluxes, T and S distribution inside and outside the Strait as well as the water residence times and the transport properties were computed to quantify the influence of tidal forcings.

The residence times were defined accordingly to Cucco and Umgiesser (2006) as a Eulerian Transport Time Scales (ETTS hereafter, Cucco et al., 2009; Cucco and Umgiesser, 2015) and computation were carried out only for the inner part of the MS, between Messina (station 10) and Capo Peloro (Faro, station 4). Two different sections inside the MS, A-B and C-D in figure 1c, were used to compute the fluxes through the Strait and to investigate the vertical variability of the main hydrodynamics.

4.1 Tidal dynamics in MS

In the TDO scenario SHYFEM was applied to reproduce the propagation of tides inside the MS and surrounding areas. The water levels computed at the tidal stations both outside (stations 1, 2 and 3 in Figure 1a) and inside the Strait (stations from 4 to 7 in Figure 1b) were compared with observations to estimate the model accuracy in predicting the tidal waves propagation in the domain.



For each station, harmonic analysis was applied to extract the amplitudes and phases of each main tidal constituent. The main harmonics observed amplitudes and phases were estimated by Vercelli, (1925) during the homonym Oceanographic cruise in 1922, and more recently reported by Brandolini et al., (1980) and Androsov et al., (2002a). In this work we refer to the values from Brandolini et al., (1980) for stations 1 to 6 and from Androsov et al., (2002a) for stations 7 to 10. We considered the tidal signal as composed by 4 semidiurnal waves (M2, S2, N2 and K2), by 3 diurnal waves (K1, O1 and P1) and by the M4 as compound tide.

In table 2 the computed and observed amplitudes and phases of the main components are reported. For stations inside the MS most of tidal energy, around 40% of the total amplitude, is contained in the M2-wave, around 19% in the S2-wave, and around the 14% of the total energy in the K1-wave. The obtained results are in line with the observed energy balance, in which M2-wave accounted for 38%, S2-wave for 16% and K1 for 13% of the total water level.

15

20

25

30



STATIONS		AMPLITUDE (cm)															
		M2		S2		N2		K2		K1		O1		P1		M4	
		m	o	m	o	m	o	m	o	m	o	m	o	m	o	m	o
1	Milazzo	12.7	12.1	5.0	4.7	2.7	-	1.6	1.3	3.6	3.2	1.2	0.9	1.0	1.1	0.0	-
2	Lipari	12.6	12.1	4.9	4.9	2.6	-	1.6	1.3	3.5	2.7	1.2	0.9	1.0	0.9	0.0	-
3	Tropea	13.5	14.6	5.0	5.2	2.6	-	1.6	1.4	3.8	4.1	1.3	1.0	1.1	1.4	0.0	-
4	Faro	7.4	5.5	2.8	3.1	1.6	-	0.9	0.8	2.3	2.3	0.7	1.0	0.6	0.8	2.4	-
5	V.S. Giovanni	2.5	3.3	1.4	1.3	0.6	-	0.4	0.3	1.5	1.2	1.0	0.2	0.5	0.4	1.2	1.9
6	Reggio C.	4.5	6.2	2.6	3.0	0.8	-	0.8	0.8	1.7	1.6	1.0	0.8	0.5	0.6	0.1	-
7	Ganzirri	4.4	3.2	1.7	1.6	1.0	-	0.5	-	1.5	1.4	0.5	0.5	0.4	-	0.5	-
8	Scylla	10.1	10.2	3.8	3.2	2.2	-	1.2	-	2.9	2.8	1.1	0.9	0.8	-	0.1	-
9	P.taPezzo	3.1	0.9	0.7	0.8	0.8	-	0.2	-	1.2	0.9	0.9	1.6	0.4	-	2.7	-
10	Messina	2.0	5.3	1.5	2.8	0.3	-	0.5	-	0.7	0.9	0.7	0.9	0.3	-	0.7	-
		PHASE (deg)															
1	Milazzo	221	262	287	287	330	-	346	287	171	222	93	126	251	222	125	-
2	Lipari	220	258	286	286	329	-	346	286	172	212	91	162	252	212	51	-
3	Tropea	218	274	283	296	327	-	349	296	168	219	95	160	247	219	329	-
4	Faro	227	269	298	314	333	-	335	314	183	232	88	251	262	232	171	-
5	V.S. Gioavnni	92	116	119	104	222	-	167	104	54	48	20	-	131	48	181	72
6	Reggio C.	49	95	97	100	176	-	179	100	25	57	6	50	108	57	357	-
7	Ganzirri	235	316	317	354	337	-	318	-	193	242	75	214	271	-	170	-
8	Scylla	215	271	281	295	324	-	352	-	163	220	81	136	243	-	167	-
9	P.taPezzo	193	143	265	137	299	-	8	-	192	236	43	235	198	-	179	-
10	Messina	36	31	83	98	182	-	193	-	220	290	14	65	110	-	24	-

Table 2: amplitude and phase of main harmonics observed (o) and computed (m) from calibrated model results in TDO scenario at the 10 tide gauge locations. Observed values for stations 1 to 6 refer to Brandolini et al., (1980) for stations 7 to 10 refer to Androsov et al., (2002a). Both authors refer to Vercelli (1925).

5

Considering the amplitude of the M2-wave, the Root Mean Square Error (RMSE, hereafter) between model results and observations computed for the whole set of stations was on average about 1.7 cm with discrepancies ranging between 0.1 cm and 3.3 cm. As for the amplitudes, also the computed phases mainly agree with observations, with average discrepancies between model results and observed values estimated to be around 40°.

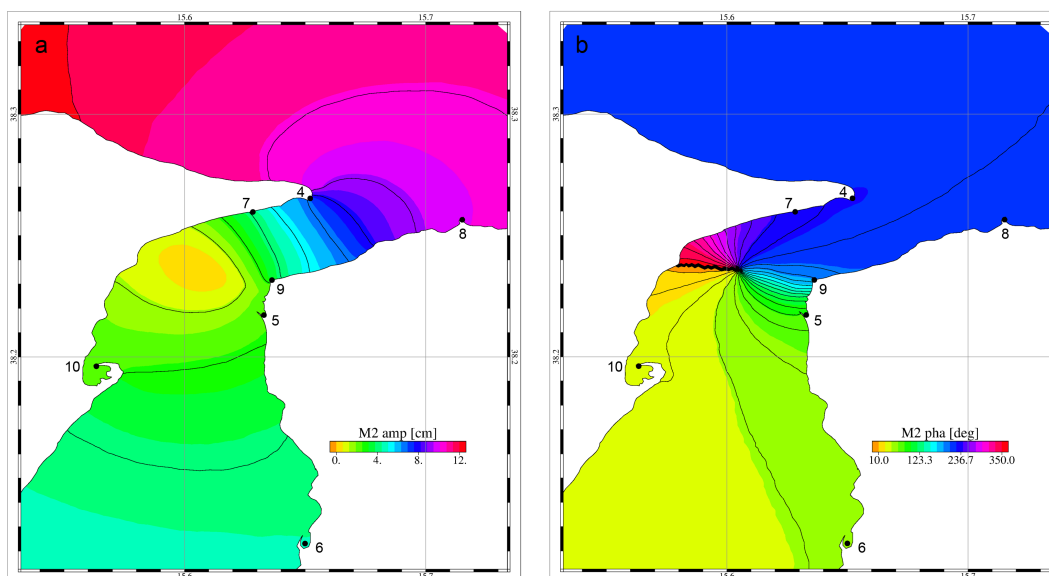
10 In Figure 2 the tidal maps of the M2-wave are reported for the MS area. The iso-phases distribution (figure 2b) highlight an anticlockwise propagation of the main semidiurnal with the presence of an amphidromic point in the middle of the Strait in correspondence of the sill in front of Punta Pezzo (station 9). The amplitudes tend to decrease from value around 11 cm



outside the Strait to values lower than 5 cm inside. This behavior was similarly described by many authors (Massi et al., 1979; Brandolini et al., 1980; Androsov et al., 2002a) confirming the accuracy of the model results in reproducing the main semidiurnal features of the tidal dynamic in the MS.

Considering the main diurnal K1, the RMSE between the observed and computed amplitudes is about 0,3 cm with values
5 varying between 0.1cm and 0.8 cm. The phases also agree with observations with average discrepancies between observed and computed values around 40°. Similarly, for the main semi-diurnal, also the tidal amplitudes of the K1 generally decrease inside the Strait even if no rotation of the tidal ellipses was found.

For the main compound tide, M4-wave, the experimental dataset was incomplete, with observations available only for station
5 (Villa S. Giovanni) on the eastern side of the MS. For this station, the computed amplitude is in line with observations with
10 an estimated discrepancy less than 1 cm. Even if not quantitatively evaluable by direct comparison with experimental data, the computed M4 amplitudes vary inside the MS following the same features described by Androsov et al., (2002a), with higher values in proximity of the sill on the eastern side of the MS (stations 9 and 5) and in proximity of Capo Peloro (station 4) on the western side of the MS.



15 *Figure 2: Tidal map of M_2 -wave in the MS and surrounding areas. iso-amplitudes in cm (panel a) and iso-phases in degrees (panel b).*



- The water circulation induced by the tides in the Strait develops mainly along the main axis of the channel, with a northward flow during the flood and southward flow during the ebb phase. Figure 3 shows the vertically averaged water current fields computed at the maximum flow during both flood (figure 3a) and ebb phases (figure 3b) of a spring tidal cycle. Numerical results evidenced how, for the sill area, the ebb flow (southward) is generally more intense than the flood flow (northward).
- 5 Along the CD section the maximum current speed computed during the spring tidal cycle was about 2.4 m/s during the ebb and about 2.1 m/s during the flood flow. Similar features were observed and reported by many authors (Massi et al., 1979; Bignami and Sallusti, 1990; Androsov et al, 2002a). In both phases, the speed variability is high and is modulated by the presence of the sill, which promotes an increase of the flow in both directions, with maximum values always found at the eastern side of the Strait in correspondence of station 6 (Punta Pezzo).
 - 10 Water fluxes computed through the section CD from the TDO scenario predicted maximum flux values of about 0.4 Sv in spring tides during ebb flows. On average, the ebb (southward) and the flood fluxes (northward) was about 0.1 Sv with differences between the two tidal phases of about 0.01 Sv, and with a dominance of southward flows.

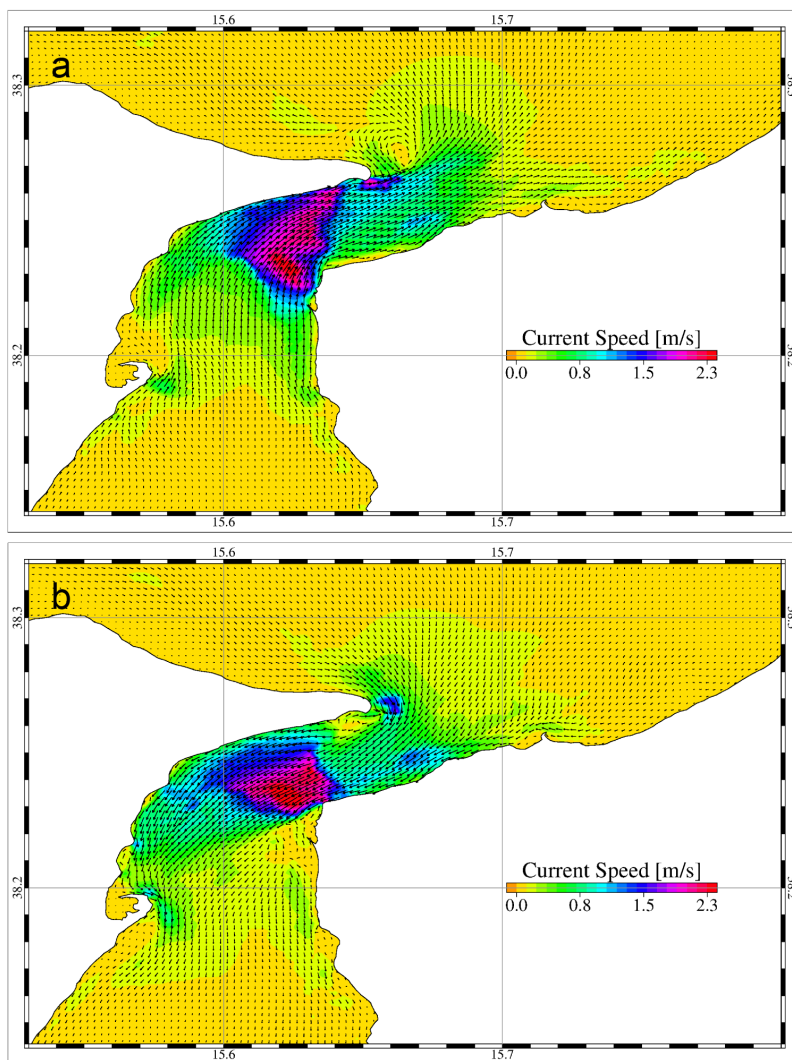


Figure 3: vertically averaged water currents fields computed at the maximum flow during ebb phase (panel a) and flood phase (panel b) of spring tides.



During maximum inflow and outflow, advective eddies are generated at the lee-side of the main capes. In particular, during the ebb phase (figure 3b) an inertial cyclonic feature is generated south of Punta Pezzo (station 8), whereas anticyclonic eddies are produced at the southern side of Capo Peloro in correspondence of Ganzirri and Faro stations (stations 4 and 7) and south to Messina harbour (station 10). On the contrary, during the maximum flood flow (figure 3a) a small cyclonic eddy is generated north of Punta Pezzo on the Calabria side whereas an intense anticyclonic eddy is produced outside of the strait by the intense outflow north of Peloro Cape. Similar inertial features were described by Cescon et al., (1997) which measured a strong inertial anticlockwise eddies south of Punta Pezzo (see figure 2 in Cescon et al., 1997) migrating from the coast to the inner Strait during the ebb flow. These features were not described by previous modelling works as in Androsov et al., (2002a) whose results highlighted only the flow vorticity generated by the bending of the Strait (see figure 12 in Androsov et al., 2002a). In that case, in fact, the low model spatial resolution was not adequate to solve the quasi-inertial features generated by the flow-morphology interactions.

During the slack phases at maximum and minimum tides the circulation pattern is less homogeneous and complicated flow geometries arise from the interaction between the out-flowing and the in-flowing water masses.

The aforementioned advective features are the main factors influencing the residual tidal flow inside the Strait. In Figure 4 the Eulerian residual current field computed for the whole set of simulated synodic months and vertically averaged is reported for the MS area.

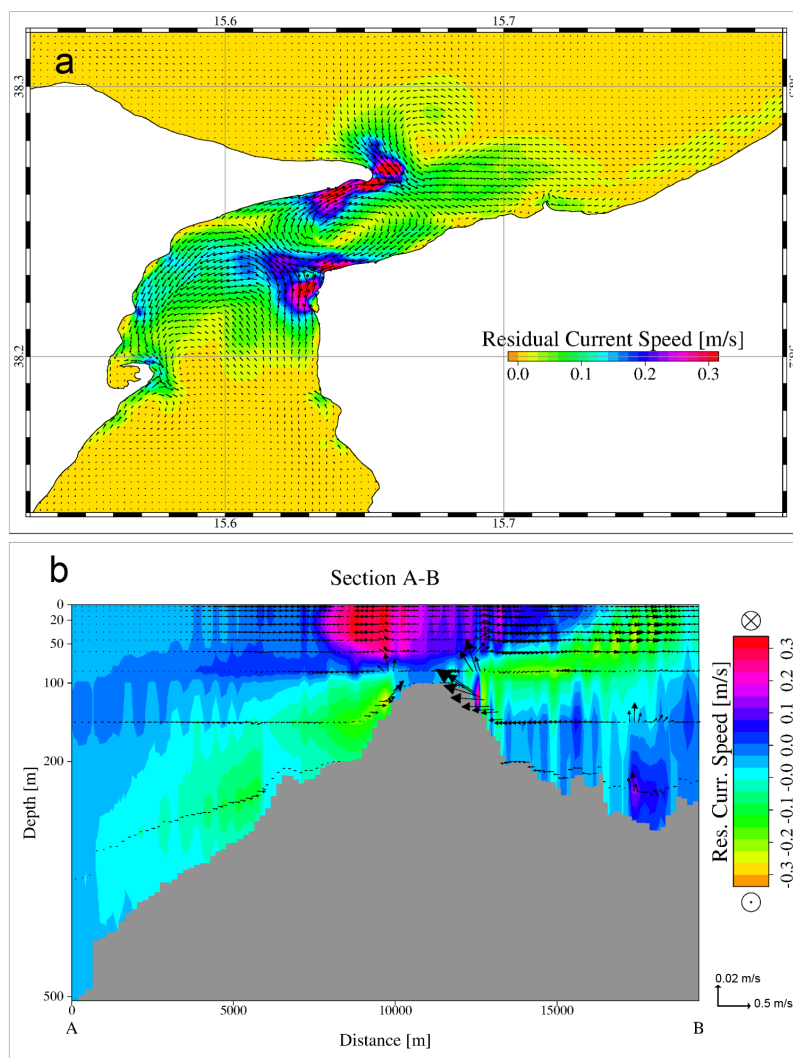


Figure 4: vertical averaged residual circulation induced by tides in MS (panel a) and residual flow across and along section A-B (panel b).



The intensities of the residual speed are not homogeneous inside the MS with values ranging between few cm/s up to 0.6 m/s in correspondence of main capes (Peloro Cape and P.ta Pezzo) and generally around 0.2 - 0.3 m/s. The computed residual speeds are in line with values found in Androsov et al., (2002a) which individuates higher values around 0.2 m/s, in correspondence of the middle of the sill and few cm/s for deeper part of the Strait. Among the presence of the several
5 cyclonic and anticyclonic structures there is also evidence of a fixed circulation pattern promoting the transfer of water masses from the Tyrrhenian Sea along the Calabrian coast to the Sicilian coast in correspondence of the sill and then, southward to the Western Ionian Sea. This was also found in Androsov et al., (2002a) and validated through empirical observations by Mosetti (1988).

Figure 4b shows the vertical distribution of the residual circulation along the section AB as computed for each model layer.
10 The residual flow is not vertically homogeneous with differences in both direction and intensity. Two main cells, converging in proximity of the sill with an upward flow on both Tyrrhenian and Ionian side, dominate the velocity components of the residual currents along the section. In particular, while the northern cell is continuous, connecting the outer deep layers to the inner surface layers, the southern cell is incomplete and characterized by the presence of convergence zone in correspondence of the surface layers close to the sill. Across the section, the residual flow is characterized by the presence of
15 an inversion of the current direction between the surface layers and the bottom layers on both side of the sill. The higher residual speeds are found within the top 50 m depth. The intertidal variability of the residual circulation is generally low with an average standard deviation of the residual current intensity of about 0.05 m/s.

4.2 The role of tides in modulating the MS general circulation

The dominant role of tidal forcing in both promoting the exchanges between the two sub-basins and modulating the
20 hydrodynamics inside the MS was evidenced by the TDO scenario results. The quantification of tidal contribution to the general circulation both inside and outside the Strait was investigated by comparing the THO (without tidal forcing) and the TTC (with tidal forcing) scenario results. In both scenarios the seasonal variation of temperature (T), salinity (S) and velocity fields in the area was reproduced. Simulations results were analysed considering typical winter and summer conditions in order to investigate the seasonal variability of the variables of interest.

25 The comparison was carried out considering the water circulation and the fluxes through the Strait, the T and S distribution and finally the ETTS and the transport dynamics as reproduced by the 2 scenarios.

4.2.1 Water circulation

Comparison between the instantaneous current fields obtained from the THO and TTC scenarios is trivial being the differences between the speeds intensities in the two cases higher than the magnitude order, with m/s obtained when
30 including the tidal forcing and cm/s when not. Therefore, analysis was carried out considering the residual flow, more suitable to quantify the influence of tides on the long term circulation patterns.



In figures 5 and 6 the residual currents computed for winter and summer seasons as the algebraic averages of the three-dimensional hourly current speeds obtained for winter and summer months are reported for both scenarios. Upper panels (a and b in figures 5 and 6) refer to the residual circulation obtained as the vertical averages of the residual velocities computed between the surface and the 50 m depth layer. Bottom panels (c and d in figures 5 and 6) refer to the residual field computed at the 100 m depth layer, which include the deepest part of the MS sill and where Tyrrhenian and Ionian deeper waters signals can be detected. Left (b and d in figures 5 and 6) and right panels (a and c in figures 5 and 6) show the results obtained without and with the tidal contribution, respectively.

10

15

20

25

30

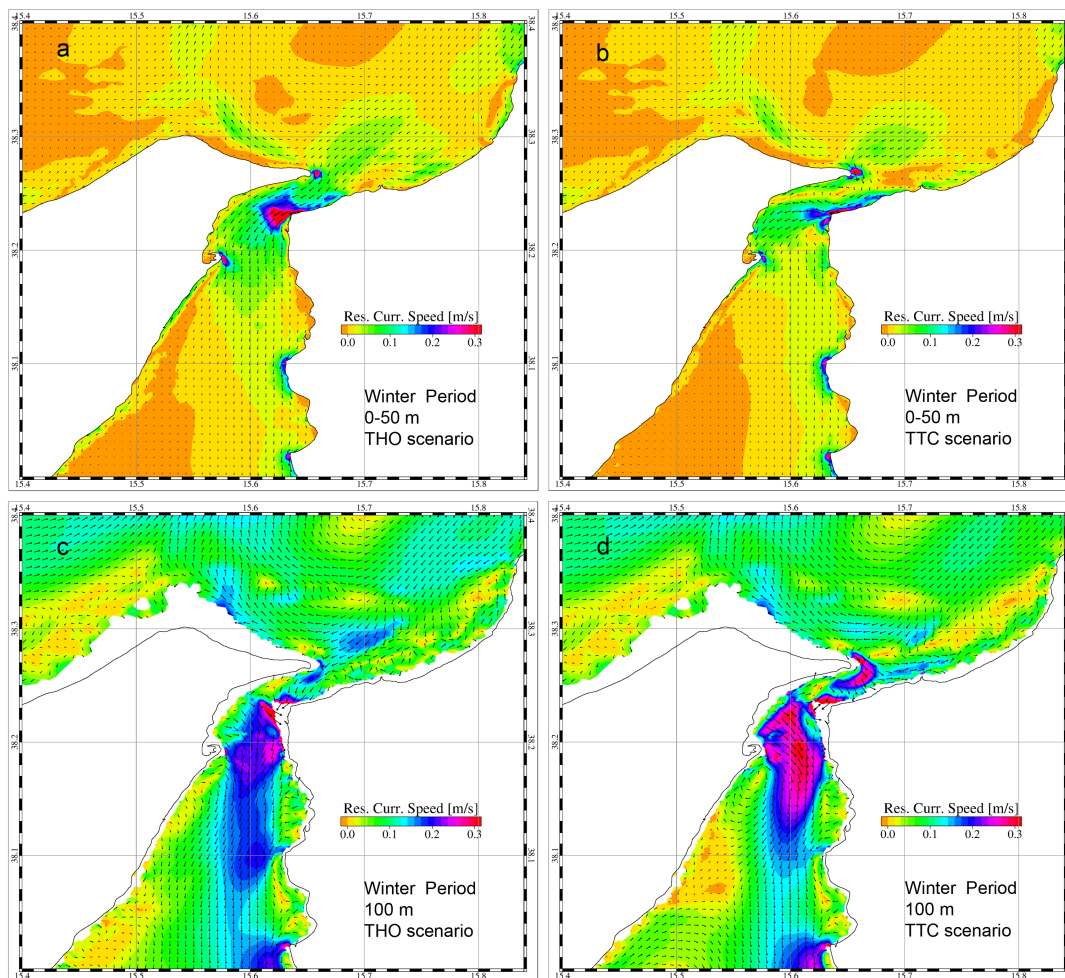


Figure 5: computed winter residual current field from the THO scenarios results (panels a and c) and from the TTC scenario results (panels b and d). Upper panels refer to average residual velocities computed between 0 and 50 m (panels a and b). Bottom panels refer to residual velocities at 100 m depth (panels c and d).

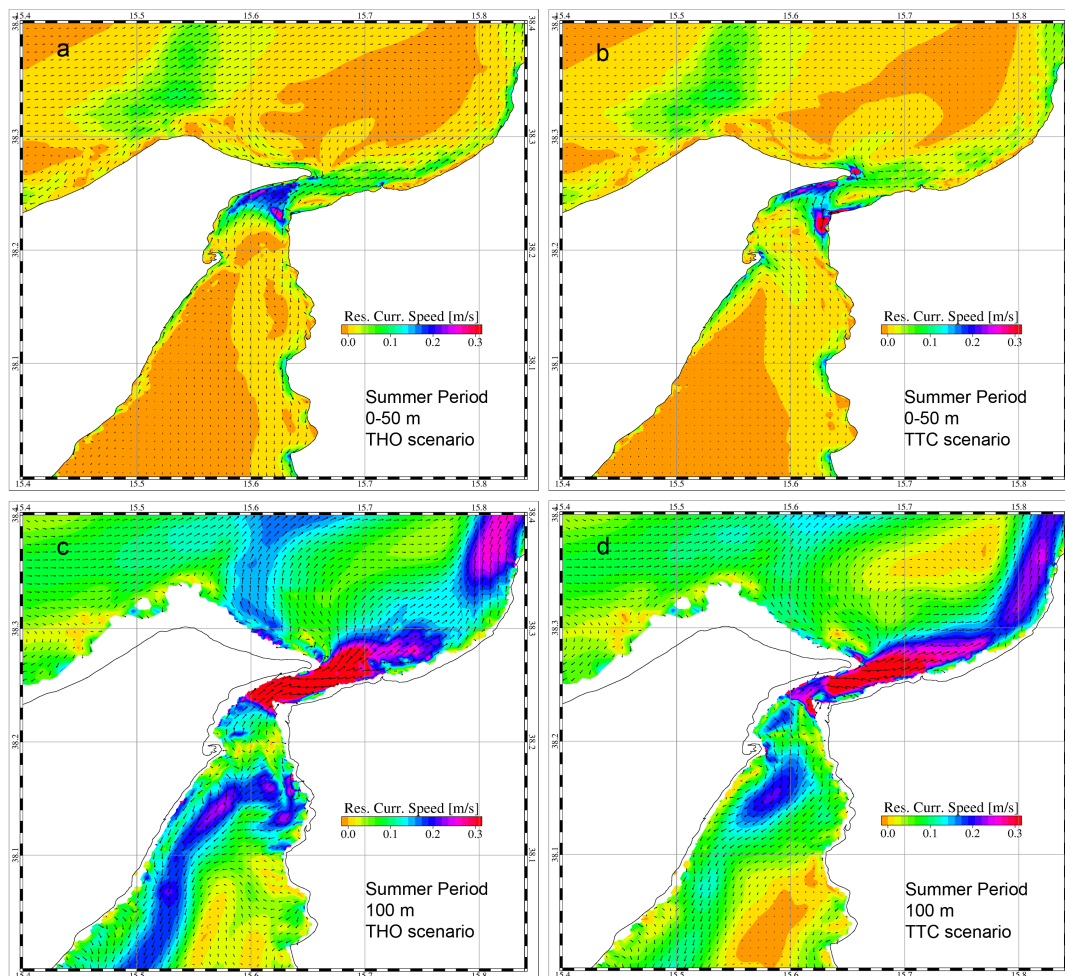


Figure 6: computed summer residual current field from the THO scenarios results (panels a and c) and from the TTC scenario results (panels b and d). Upper panels refer to average residual velocities computed between 0 and 50 m (panels a and b). Bottom panels refer to residual velocities at 100 m depth (panels c and d).

5

Inside the MS, during the winter period, the wind and thermohaline forcings only (THO scenario) promote a residual circulation mainly homogeneous in space and directed southward with average speeds around 0.1 m/s (figure 5a). Local intensifications are found in correspondence of the main capes and on the eastern side of the sill where a residual speed up to



0.6 m/s is detected at the surface layers. At 100 m depth (figure 5c), the residual current field is generally more intense than at the surface, with average values higher than 0,2 m/s and peak values of 0,68 m/s. The deeper residual flow is also directed southward with a more homogeneous pattern found in the southern part of the MS.

Considering the TTC scenario results, the surface residual circulation obtained for winter months (figure 5b) is strongly modulated by the residual tidal current field (figure 3a) promoting the generation of anticyclonic and cyclonic gyres within the Strait. Similar values, around 0,6 m/s, were found for the surface peak speeds. Contrary, in the deeper layers, the action of tidal forcing, while preserving the current pattern generated by the wind and heat fluxes, tends to promote a general increment of the average residual speed intensities, which, in this case, are higher than 0,3 m/s. Outside the MS, both in the Tyrrhenian and Ionian sides, the action of the tides tends to reduce the residual speeds intensities and to increase the number of small scales gyres generated at the MS mouths. As we expected, the differences in the open ocean residual fields due to the tidal contribution are generally low and tend to be reduced with the distance from the MS.

During the summer period, the wind induced and thermohaline residual circulation (THO scenario) at the surface (figure 6a) is less intense with peak speeds around 0.3 m/s and, contrary to winter period, is directed northward in the northern part of the Strait and southward in the southern part. The same pattern is found at the deeper depths where a stronger residual flow, up to 0.7 m/s, rising at the sill moves northward into the Tyrrhenian Sea and, bending eastward generates a coastal current on the Calabria side. In the southern opening of the MS, the southward flow is less intense, around 0.2 m/s, and mainly confined to the western side of the Strait. In both, surface and deeper layers, a divergence area is detected south of the sill in front of the Messina harbour (station 10).

As for the winter period, when tidal forcing is included (TTC scenario), the surface residual current pattern inside the MS (figure 6b) differs mainly for the presence of anticyclonic and cyclonic structures generated by the residual tidal flow. A general reduction of the residual current speeds is recorded at both surface and deep layers and both inside and outside the MS. In this case, the tidal action, while preserving the general pattern, tends to modify the two main residual flows, the northward and southward one, both inside and outside the MS. This is particularly evident at the 100 m depth layer outside the MS in the Tyrrhenian Sea (figure 6d), where the coastal current along the Calabria side is stronger and sharper than the one obtained from THO scenario results (figure 6c). On the contrary, in the Ionian waters, the tidal forcing tends to disrupt the southward coastal flow by reducing its maximum speed and by smoothing the horizontal velocity gradients. Finally, the tidal action reduces the extension of the divergence areas inside the MS at both surface and deeper depths.

Water fluxes through section CD, computed for 45 days during both winter and summer periods from the THO and TTC scenarios results are reported in figure 7. The hourly data highlight the different magnitudes of the computed fluxes between the two scenarios, with peak values higher than 0.4 Sv obtained when including the tides (blue lines in figure 7a and 7b) and values always less than 0.2 Sv when not (red lines in figure 7a and 7b). As expected, the differences between the TTC and the THO net fluxes are always different from 0. This is evident when considering the 24-hours mobile averages computed from the TTC results (black line in figure 7a and 7b) where values, even if generally following the trend, are always differing from the computed THO fluxes. For both scenarios, winter and summer time series differ mainly for the net flux



budget between inflows and outflows where values are generally negative, during winter time, indicating a southward average flow, and positive in summer, indicating a northward flow.

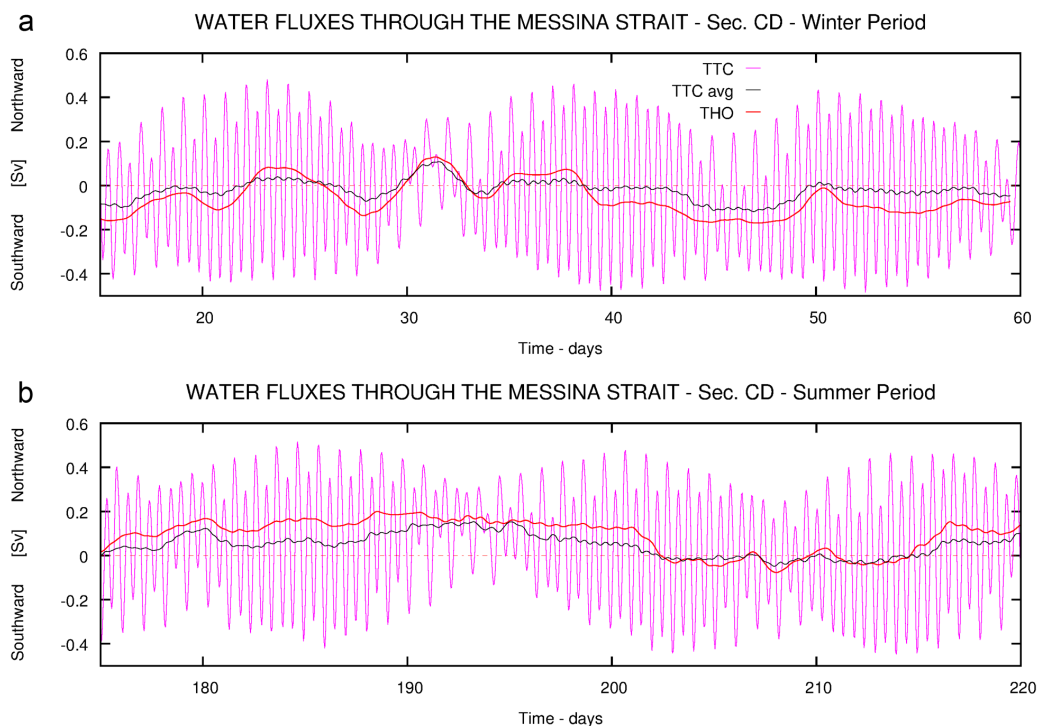


Figure 7: water fluxes through section CD computed for 45 days during winter (panel a) and summer periods (panel b) from THO scenario results (red line) and from TTC scenario results (blue line for hourly data, black line for daily data), units are expressed in Sv with negative values indicating southward flux (ebb flow) and positive a northward flux (flood flow)

In table 3 the average positive, negative and net fluxes computed during the winter and summer periods are reported for both scenarios. Also in this case, the differences between the THO and TTC results are found for both the northward and the southward fluxes, with TTC average values always greater than THO ones, with values ranging between 0.084 Sv and 0.04 Sv. This is particularly clear for the winter period when the less intense density gradients, leading to a lower contribution to the general circulation, tends to increase the differences between the two scenarios.



From both scenarios, the computed net flux is negative (southward) in winter and positive (northward) in summer, with tidal forcing that tends to smooth these discrepancies (TTC-THO in table 3) with a reduction of 0.042 Sv to the net southward flux in winter and a reduction of 0.039 Sv to the net northward flux in summer.

Water flux through section C-D (units expressed in Sv)				
Season	Scenario	Net Flux (N-S)	North Flux	South Flux
Winter	TTC	-0.022	0.097	0.120
	THO	-0.065	0.014	0.080
	<i>TTC-THO</i>	<i>0.042</i>	<i>0.082</i>	<i>0.040</i>
Summer	TTC	0.052	0.131	0.078
	THO	0.092	0.101	0.008
	<i>TTC-THO</i>	<i>-0.039</i>	<i>0.029</i>	<i>0.069</i>
Salt flux through section C-D (units expressed in Sv)				
Season	Scenario	Net Flux (N-S)	North Flux	South Flux
Winter	TTC	-0.846	3.755	4.601
	THO	-2.493	0.565	3.058
	<i>TTC-THO</i>	<i>1.646</i>	<i>3.189</i>	<i>1.542</i>
Summer	TTC	2.051	5.044	2.992
	THO	3.355	3.892	0.337
	<i>TTC-THO</i>	<i>-1.503</i>	<i>1.151</i>	<i>2.655</i>
Heat flux through section C-D (units expressed in 10 ⁷ W)				
Season	Scenario	Net Flux (N-S)	North Flux	South Flux
Winter	TTC	-2.775	11.767	14.543
	THO	-7.927	1.770	9.697
	<i>TTC-THO</i>	<i>5.151</i>	<i>9.997</i>	<i>4.845</i>
Summer	TTC	6.387	15.887	9.500
	THO	11.195	12.278	1.082
	<i>TTC-THO</i>	<i>-4.807</i>	<i>3.609</i>	<i>8.417</i>

Table 3: Water, salt and heat fluxes through section CD computed for winter and summer periods from THO and TTC scenario results and differences (TTC-THO). Water and salt fluxes are expressed in Sv, heat fluxes in 10⁷ Watt. Positive net flux values indicate a northward net flux, negative values indicate a southward net flux.



4.2.2 Thermohaline features

The temporal and spatial variability of water salinity and temperature were computed for both the TTC and THO scenarios and for the whole considered period. The thermohaline properties of water masses were also analysed for the winter and summer seasons similarly to the dynamical features.

- 5 From the TTC scenario results, the vertically averaged salinity in the MS area varied between 37.7 PSU, for the Tyrrhenian waters in the northern part, and 38.6 PSU, for the Ionian waters in the southern side, with average differences between winter and summer periods of about 0.5 PSU. The variation of the salinity fields due to the tidal contribution in the MS is, on average, less than 0.2 PSU with a general increment of salty water during summer and a decrease during winter period.

- 10 Figure 8 shows the winter and summer average salinity distributions computed from the THO and the TTC scenario results along the section. In winter period (figure 8a and 8b) due to the negative net flux budget across the Strait, which indicate a prevailing southward flow, the saltier Ionian deep waters are mainly confined to the southern side of the sill. The action of tides, favouring the exchanges at the interface, tends to promote the outflow of saltier Ionian deep waters on the northern side of the Strait (figure 8b). This is confirmed by the computation of the average salt net fluxes through section CD (table 3) that indicates a general decrease of the southward flux component, estimated around 1.6 Sv, when considering the tidal contribution. The differences in the vertical structures between the two scenarios are mainly due to the tidal residual current field, that follows a pattern, characterized by a convergence in proximity of the sill (figure 3b), that tends to foster the rising of deeper and saltier waters.

- 15 In summer period, the average northward net flux (table 3) causes the partial overflow of the Ionian lower surface waters across the sill into the northern side of the MS. While tidal exchanges generally tends to counteract this process, as confirmed by the negative differences of -0.039 Sv between the net fluxes in the two scenarios (table 3), the tidal residual flow promotes a general increment of the salinity on the northern side of the sill. This is confirmed by the ratio between the the TTC and THO net fluxes which, in case of water fluxes is around 0.56 and in the case of salt fluxes is slightly higher up to 0.61 (table 3, 2.051 Sv in the TTC scenario versus 3.355 Sv obtained for the THO scenario), therefore indicating that horizontal flow as not the only factor regulating the salt budget through the section.

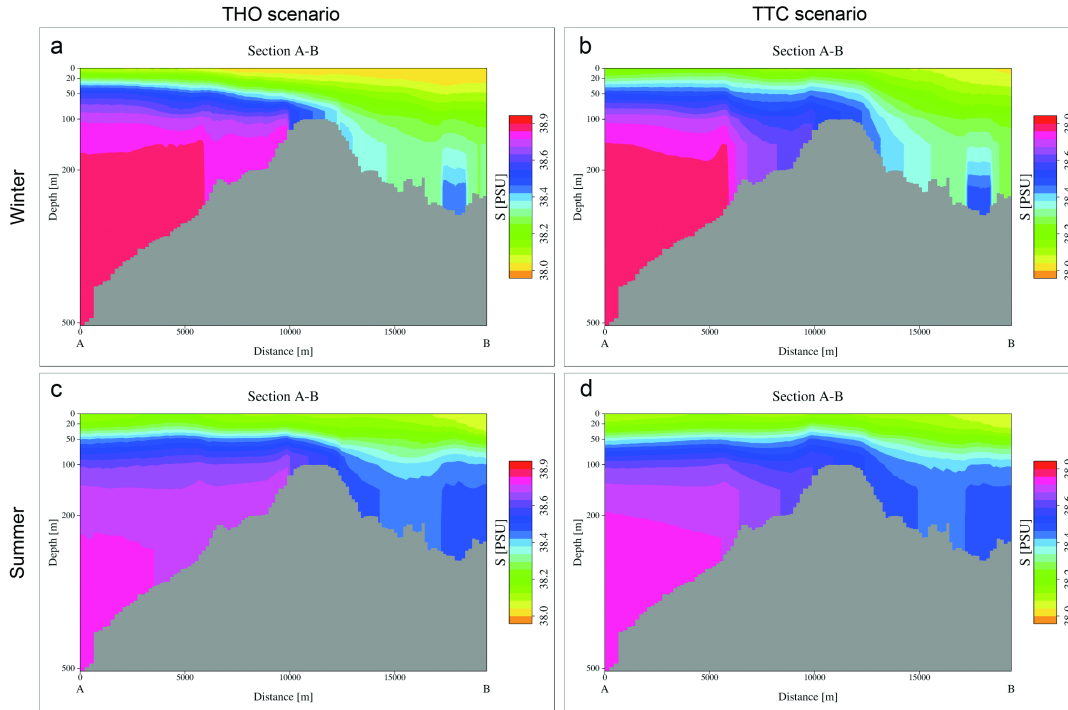


Figure 8: vertical distribution of the average water salinity expressed in PSU computed along the section AB from THO (panels a and c) and TTC scenario results (panels b and d) for winter (panels a and b) and summer periods (panels c and d).

5 During winter water T in the area is mainly homogeneous ranging between 14°C and 17°C with average values around 14.5°C and small variations in the vertical due to the absence of thermal stratification and to the strong mixing. During this period, the effects of tidal action in changing the T fields are negligible with differences between the THO and TTC scenarios around 0.1°C and 0.2°C.

10 During summer, due to the strong heat fluxes and the intense large scale thermohaline circulation, the T distribution in the area is heterogeneous both horizontally and vertically. In figure 9a the average surface T computed from the TTC scenario results is reported for the extended domain comprising the MS and part of the two sub-basins. The values vary between 19°C and 26°C with the lowest T found in the MS, south to the sill, and higher values found in the shallow water banks on both the Tyrrhenian and Ionian coastal areas. The computed T distribution is in line with measurements carried out by Cescon et al., (1997) who individuated cores of cold waters inside the MS both south to the sill and south to the Messina harbour on the
 15 Sicilian side of the Strait (see figure 7 in Cescon et al, 1992). During this period, the tides, modifying the instantaneous and



the residual flow pattern and increasing the mixing processes at the interfaces, cover an important role in shaping the surface T fields in the area.

In figure 9b the differences between the average surface T computed from TTC and THO scenarios are reported. For the offshore fields, in both the Tyrrhenian and Ionian Sea, where the T variability is mainly ruled by the large scale thermohaline circulations, the changes due to tidal action are negligible. On the other hands, significant differences due to tidal action are found inside the Strait where a decrease of T, up to 1°C , is detected and outside, along the coastal areas, where a general increment of the T is found when tides are included.

Inside the MS, the tides tend to reduce the surface T in proximity of the sill with the consequent increase of the model prediction accuracy, as suggested by the comparison with the experimental dataset obtained by Cescon et al (1997). In fact, model results obtained from the THO scenario not including the tidal action, foresee the minimum T areas in front of Reggio Calabria (station 11) and south to the Strait, whose patterns are not found in the experimental dataset. Off the northern mouth, in the Tyrrhenian Sea, the tides induce an average increase of T, up to 0.8°C , at the surface waters carried by the northward coastal current along the eastern side of the sub-basin. Similarly, in the Ionian side of the Strait, the T computed from TTC scenario results are generally higher than ones from the THO scenario, with increments ranging between 0.3° up to 1.4°C and highest differences found along both the Sicilian and Calabria coasts.

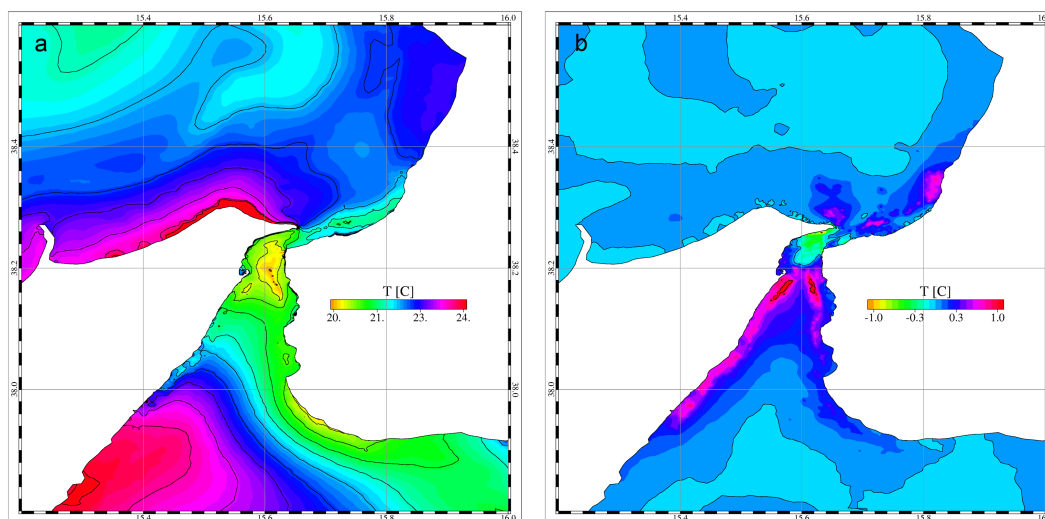


Figure 9: Surface water temperature computed during summer period, average values from the TTC simulation results (panel a) and differences with respect to the THO scenarios results (panel b).



The vertical distributions of the average summer T along the section AB (figures 10a and 10b) as computed from both scenario results, highlight the pronounced thermal stratification due to the intense heat fluxes. T values range between 14°C for the lower surface Tyrrhenian and Ionian waters and 22° C for the surface waters. Similarly to the salinity fields (figure 8d), in correspondence of the sill, the tides (figure 10b) promote the uplift of the isotherms with a consequent general reduction of the T along the water column. A general decrease in T is also found for the whole northern side of the section especially in the deeper layers where the residual circulation induced by tides tends to promote the displacement of deeper and colder Tyrrhenian waters toward the surface.

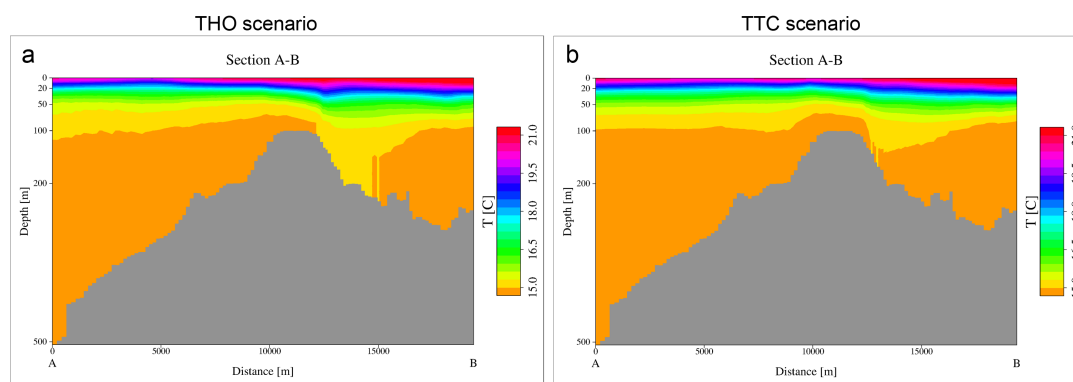


Figure 10: summer average water temperature along section AB computed from THO and TTC scenarios (panel b and d).

10

The heat budget through section AB was computed for both summer and winter periods (see table 3) revealing in the Tyrrhenian basin an average net heat loss of about 2.7×10^7 W during winter and an average heat gain during summer of around 6.4×10^7 W, as estimated from TTC scenario. The action of tides tends to reduce the discrepancies between northward and southward flows with a contribution was similar to the one found in the analysis of the water fluxes. In fact, the ratios between the TTC and the THO net values are about 0.35 for the winter period (table 3, -2.7×10^7 W in the TTC scenario versus -7.9×10^7 obtained for the THO scenario) and 0.57 for the summer period (table 3, 6.3×10^7 in the TTC scenario versus -11.2×10^7 obtained for the THO scenario), which are similar to the values found for the water net fluxes, with 0.34 and 0.56 respectively, thus indicating the changes in horizontal advection as the main factor ruling the heat balance at the interface.

15

4.2.3 Transport processes

The transport of water masses through the MS is a fundamental process to be investigated in order to understand the importance of this narrow passage on the hydrodynamics of the surrounding open and coastal seas areas.

20



With this aim, the ETTS were computed for both the THO and TTC scenario. The results obtained for the whole simulated period indicated ETTS values always lower than few days. Being this time interval not compatible with a seasonal based analysis, only the yearly average of the ETTS were considered.

In figure 11, the vertically averaged ETTS computed for the THO (panel a) and TTC (panel b) scenarios are reported. In
5 both cases values range between few hours in proximity of mouth to around 2 days in proximity of the coasts. As expected the effect of tidal forcing consists in both the reduction of the transport times and the changes in its relative distribution. Average and maximum ETTS varies from 0.51 and 1.97 days in the THO scenario to 0.34 and 1.68 days in the TTC scenario with a general decrease of about the 33% due to tides. The differences between ETTS in the two scenarios are in line with differences between the computed residual speeds intensities (see section 4.2.1). In fact, even if the instantaneous tidal
10 flushing is intense, it promotes a strong reduction of ETTS only in proximity of the mouths where waters are moved out of Strait within the first 6 hours. On the contrary, for most of the MS, the residual flow is the main forcing shaping the ETTS pattern. In fact, while in the THO scenario, the ETTS tend to increase in correspondence of the sill, with a relative maximum of about 0.6 days, in the TTC scenario the relative maximum is found south to the sill and with lower values of around 0.4 days. This shift is due to the tidal residual circulation (figure 3b) that, in correspondence of the southern part of the sill, is
15 characterized by a convergence of the residual velocities tending to create a trapping area.

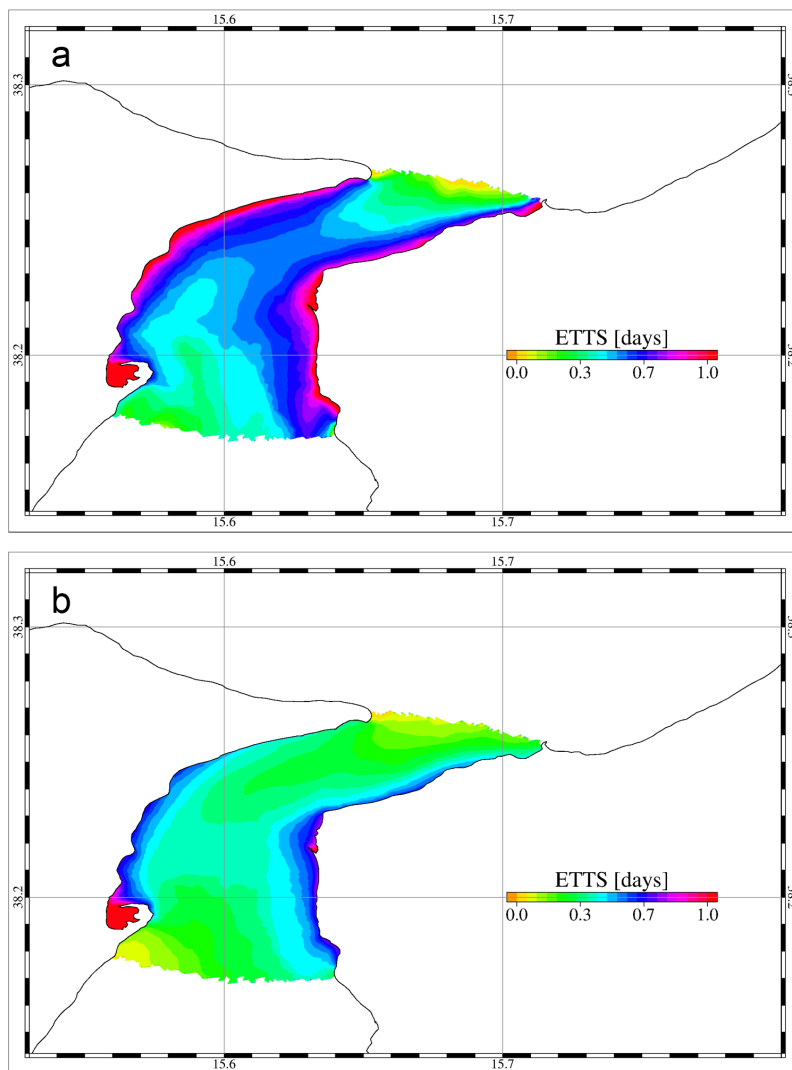


Figure 11: vertically averaged ETTS in the MS computed from the THO scenario results (panel a) and the TTC scenario results (panel b).



The effects of tidal action on the exchanges in the MS were finally evaluated considering its role in changing the dominance of Tyrrhenian and Ionian waters in the Ionian and Tyrrhenian sub-basins, respectively. Specifically, passive tracers were monthly released with unitary concentration in the southern part of the MS, south to station 10, for tracking Ionian waters, and in the northern part of the basin, north to stations 4 and 8, for tracking Tyrrhenian waters. The trajectories of both tracers were simulated for the whole considered period in both TTC and THO scenarios. The winter and the summer monthly average distribution of the tracer [C] were then analysed. In figure 12, the 0.1 [C] contour lines for the surface (5 m depth) and bottom layers are reported for both the Tyrrhenian (blue and red lines in figure 12) and Ionian tracers (green and yellow lines in figure 12) and for winter (figures 12a and 12b) and summer (figures 12c and 12d) as obtained from the THO and TTC scenarios (figures 12a and 12c).

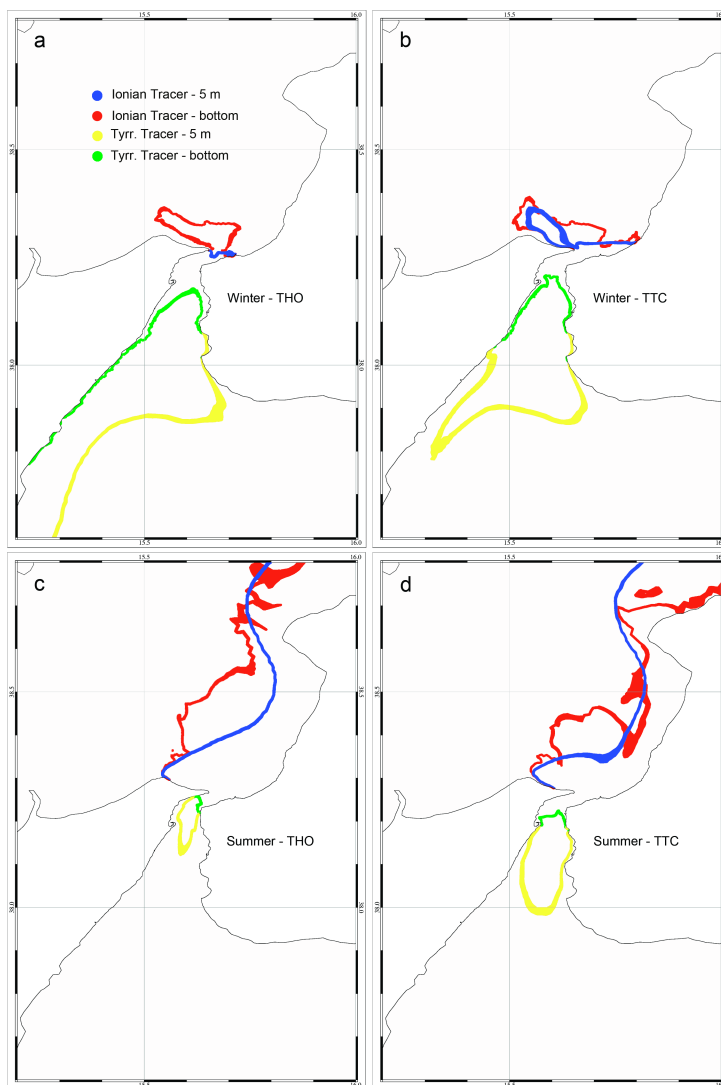


Figure 12: monthly average distribution of tracers release during winter (upper panels) and summer (lower panels) from THO (left panels) and TTC scenario results (right panels). Coloured areas refer to values with 10% the initial tracer concentration. Red and blue lines refer to Ionian tracked waters at bottom and surface layers. Green and yellow lines refer to Tyrrhenian tracked bottom and surface layers water.

5



The 10% contour lines for both surface and bottom layers indicate that during winter (figures 12a and 12b), tidal action promotes the outflow of Ionian waters into Tyrrhenian Sea and tends to reduce the presence of Tyrrhenian waters into the Ionian Sea. For both tracers, the highest variations between the two scenarios are found in the surface waters. In particular, for Ionian tracer, the tides increase the surface with an average [C] of about 14% for surface layer and about the 3% for bottom layer. Similarly, the reduction of the area with Tyrrhenian tracer [C] greater than 10% is higher for surface waters, with about the -40%, and lower for bottom layers with about the -10%. For both tracers the maximum differences induced by the tides are confined within the first 200 m, corresponding to the bathymetric threshold imposed by the sill depth.

On the contrary during summer (figures 12c and 12d), the contour lines indicate that tidal forcing promotes the outflow of Tyrrhenian waters into the Ionian Sea and tends to foster the propagation of Ionian waters northward. In particular, for Ionian waters, the reduction of the surface with tracer [C] greater than 10% was higher in deeper layers, up to 40% at the 200 m depths, and lower for surface layers, about 19% at 5 m depth. This is in line with the results obtained by the analysis of the residual circulation (figure 6b), in fact, the tidal action while reducing the residual current fields in the area, tends to maintain and promote the intense coastal current on the eastern side of the basin. This is evidenced by the fact that in case of tide, even if the 10% contour lines is less extended, the average tracer [C] in the surface layers of the Calabria coastal areas are always higher than those found in the THO scenario. On the contrary, for the Tyrrhenian tracer, the increment of the area with [C] higher than 10% induced by the tidal action, is higher for surface layers, around 35% at 5 m, and lower for deeper layers, 5% at 100 m.

5 Conclusions

The focus of this work was the investigation of the effects of reproducing tidal dynamics on modeling the general circulation in the Messina Strait, a narrow passage connecting the Tyrrhenian and the Ionian Sea sub-basins in the Western Mediterranean Sea.

The adopted approach highlighted the role of the tides in modulating the local circulation patterns and allowed to quantify the effects of the Strait tidal hydrodynamics on the circulation of the surrounding coastal waters. These aspects are particularly important when dealing with operational oceanography systems designed to provide short term predictions that, in turn, can be used by other end-users applications as Decision Support Systems (DSS) for maritime safety (Mannarini et al. 2016, this issue) or simply to provide basic fields for marine forecasting applications.

These operational oceanographic systems are generally characterized by low spatial resolution, in the order of some kms, which is too coarse to reproduce the tidal dynamics and the general circulation inside this narrow passage. As a consequence, these systems are also not suitable to make prediction over a large extent of the surrounding open sea areas where the influence of the Strait dynamic was found to be important. For this area, in fact, the correct reproduction of the MS tidal



dynamics deeply impacts on the prediction of the instantaneous and residual circulation pattern, of the thermohaline properties and transport dynamics.

Considering the exchanges between the two sub-basins through the MS, the correct reproduction of tidal dynamics in the Strait can generate changes in water fluxes ranging between 800%, when considering the instantaneous values, and 60% if
5 estimated from the residual flows. While these values are slightly influencing the overall flux budgets of the two sub-basins, the increase in current speeds in the Strait due to tides, as well as the intensification of interactions between water masses with different thermohaline properties, led to intense modifications of the current and thermohaline fields in Tyrrhenian, Sicily channel and Southern Ionian coastal waters. In fact, considering the Tyrrhenian and Sicily Channel water mass budgets, while the net fluxes through the MS are up to 2 orders of magnitude lower than the monthly average fluxes through
10 the Sardinian and Sicily Straits, with 10^{-2} Sv (table 3) and 1 Sv (Beranger et al., 2005) respectively, the instantaneous fluxes through the MS, with average values up to 10^{-1} Sv (see table 3) and maximum values around 0.5 Sv (figure 5) are comparable with the fluxes through the other boundaries (Beranger et al., 2005), therefore influencing substantially the thermohaline features of the two sub-basins.

This is particularly evident from the water temperature analysis in the outer coastal areas, where a correct reproduction of the
15 MS dynamics led to changes in surface T distribution over an external area of about 1500 km² extending up to 60 km from the Strait. Finally, considering potential oil spill or dissolved pollutant contamination, the correct reproduction of the tidal dynamics in the MS generated substantial differences in the transport patterns in the area. The analysis of transport properties revealed that, on a monthly time scale, the difference in the sea surface area interested by an hypothetical continuous release in the MS is up to 40% between the two scenarios.

20 The obtained results confirmed the importance of reproducing correctly the MS dynamics even when focusing on predicting the hydrodynamics of the external sea areas. This is not only the case of Messina Strait and Tyrrhenian and Ionian Sea and Sicily Channel sub-basins, in fact, most of open ocean operational systems applied to areas with complicated geometry, including narrow passages and straits, are not suitable to correctly reproduce the hydrodynamics of coastal waters and consequently their role in influencing the open ocean current pattern. In our study case, the water circulation inside the Strait
25 was particularly important in shaping the outer seas current patterns and thermohaline features. Therefore, the use of numerical procedures including both open ocean and high resolution coastal hydrodynamic models is warmly suggested even for operational oceanographic systems focused on predicting the open ocean hydrodynamic fields.

Acknowledgement

This research was funded by the project TESSA (Technologies for the Situational Sea Awareness) project funded by the
30 Italian Ministry for Environment.



References

- Androsov, A. A., Kagan, B. A., Romanenkov, D. A., & Voltzinger, N. E. (2002a). Numerical modelling of barotropic tidal dynamics in the strait of Messina. *Advances in Water Resources*, 25(4), 401–415. [http://doi.org/http://dx.doi.org/10.1016/S0309-1708\(02\)00007-6](http://doi.org/http://dx.doi.org/10.1016/S0309-1708(02)00007-6)
- 5 Androsov, A. A., Voltzinger, N. E., & Romanenkov, D. A. (2002b). Simulation of three-dimensional baroclinic tidal dynamics in the strait of Messina. *Izvestiya - Atmospheric and Ocean Physics*, 38(1), 105–118.
- Astraldi M. and Gasparini G.P., 1994. The seasonal characteristics of the circulation in the Tyrrhenian Sea, In: Seasonal and interannual variability of the western Mediterranean Sea, Coastal and Estuarin Studies Series, AGU, 46, 115-134
- 10 Bellafiore, D., Umgiesser, G., & Cucco, A. (2008). Modeling the water exchanges between the Venice Lagoon and the Adriatic Sea. *Ocean Dynamics*, 58(5-6), 397–413.
- Bellafiore, D., Guarnieri, A., Grilli, F., Penna, P., Bortoluzzi, G., Giglio, F., & Pinardi, N. (2011). Study of the hydrodynamical processes in the Boka Kotorska Bay with a finite element model. *Dynamics of Atmospheres and Oceans*, 52(1–2), 298–321. <http://doi.org/http://dx.doi.org/10.1016/j.dynatmoce.2011.03.005>
- 15 Béranger, K., Mortier, L., & Crépon, M. (2005). Seasonal variability of water transport through the Straits of Gibraltar, Sicily and Corsica, derived from a high-resolution model of the Mediterranean circulation. *Progress in Oceanography*, 66(2–4), 341–364. <http://doi.org/http://dx.doi.org/10.1016/j.pocean.2004.07.013>
- Bossolasco, M. & Dagnino, I., (1957). Sulla turbolenza delle correnti marine nello Stretto di Messina. *Geofis. Pura e Appl.*, 37, 318-324.
- 20 Bossolasco, M. & Dagnino I., (1959). La diffusione delle acque ioniche nel Tirreno attraverso lo Stretto di Messina. *Geofis. Pura e Appl.*, 44, 318-324.
- Brandt, P., Rubino, A., Alpers, W., & Backhaus, J. O. (1997). Internal Waves in the Strait of Messina Studied by a Numerical Model and Synthetic Aperture Radar Images from the ERS 1/2 Satellites. *Journal of Physical Oceanography*, 27(5), 648–663. [http://doi.org/10.1175/1520-0485\(1997\)027<0648:IWITSO>2.0.CO;2](http://doi.org/10.1175/1520-0485(1997)027<0648:IWITSO>2.0.CO;2)
- 25 Brandt, P., Rubino, A., Quadfasel, D., Alpers, W., Sellschopp, J., & Fiekas, H.-V. (1999). Evidence for the Influence of Atlantic–Ionian Stream Fluctuations on the Tidally Induced Internal Dynamics in the Strait of Messina. *Journal of Physical Oceanography*, 29(5), 1071–1080. [http://doi.org/10.1175/1520-0485\(1999\)029<1071:EFTIOA>2.0.CO;2](http://doi.org/10.1175/1520-0485(1999)029<1071:EFTIOA>2.0.CO;2)
- Burchard, H., & Petersen, O. (1999). Models of turbulence in the marine environment —a comparative study of two-equation turbulence models. *Journal of Marine Systems*, 21(1–4), 29–53. [http://doi.org/http://dx.doi.org/10.1016/S0924-7963\(99\)00004-4](http://doi.org/http://dx.doi.org/10.1016/S0924-7963(99)00004-4)
- 30 Blumberg, A. F., & Mellor, G. L. (1987). Three dimensional shelf models. *Coastal Estuarine Science*, , 1-16
- Carta G., D'Epifanio R. & Monti S. (2008). Le Correnti di Marea nello Stretto di Messina, Technical Report, Istituto Idrografico della Marina, Genova, 43



- Cescon, B., Azzaro, F., Creazzo, S., Decembrini, F. & Magazzu, G. (1997). Processes affecting upwelling and primary productivity of the Messina Straits. *Bollettino di Geofisica Teorica ed Applicata*, 38, 1-2.
- Coiro D, Troise G, Ciuffardi T & Sannino G, (2013). editors. Tidal current energy resource assessment: The Strait of Messina test case. *Clean Electrical Power (ICCEP)*, 2013 International Conference on; 2013: IEEE
- 5 Cucco, A., & Umgiesser, G. (2006). Modeling the Venice Lagoon residence time. *Ecological Modelling*, 193(1–2), 34–51. <http://doi.org/http://dx.doi.org/10.1016/j.ecolmodel.2005.07.043>
- Cucco, A., Umgiesser, G., Ferrarin, C., Perilli, A., Canu, D. M., & Solidoro, C. (2009). Eulerian and lagrangian transport time scales of a tidal active coastal basin. *Ecological Modelling*, 220(7), 913–922. <http://doi.org/10.1016/j.ecolmodel.2009.01.008>
- 10 Cucco, A., Sinerchia, M., Ribotti, A., Olita, A., Fazioli, L., Perilli, A., ... Sorgente, R. (2012). A high-resolution real-time forecasting system for predicting the fate of oil spills in the Strait of Bonifacio (western Mediterranean Sea). *Marine Pollution Bulletin*, 64(6), 1186–200. <http://doi.org/10.1016/j.marpolbul.2012.03.019>
- Cucco, A., & Umgiesser, G. (2015). The Trapping Index: How to integrate the Eulerian and the Lagrangian approach for the computation of the transport time scales of semi-enclosed basins. *Marine Pollution Bulletin*, 98(1), 210–220.
- 15 Defant, A., 1940. Scilla e Cariddi e le correnti di marea nello Stretto di Messina. *Geopis. Pura e Appl.*, 2, 93-112.
- Defant, A., 1961. *Physical Oceanography*. 1, 2. Pergamon Press, Oxford – London - New York – Paris, 1327
- Dobricic, S. and Pinardi, N.: An oceanographic three-dimensional variational data assimilation scheme, *Ocean Modell.*, 22, 89–105, doi:10.1016/j.ocemod.2008.01.004, 2008.
- Fazioli, L., Olita, A., Cucco, A., Tedesco, C., Ribotti, A., & Sorgente, R. (2016). Impact of different initialisation methods on the quality of the sea forecasts for the Sicily Channel. *Journal of Operational Oceanography*. <http://doi.org/10.1080/1755876X.2015.1114804>
- 20
- Ferrarin, C., Roland, A., Bajo, M., Umgiesser, G., Cucco, A., Davolio, S., ... Drofa, O. (2013). Tide-surge-wave modelling and forecasting in the Mediterranean Sea with focus on the Italian coast. *Ocean Modelling*, 61, 38–48. <http://doi.org/http://dx.doi.org/10.1016/j.ocemod.2012.10.003>
- 25 Ferrarin, C., Bajo, M., Bellafiore, D., Cucco, A., De Pascalis, F., Ghezzi, M., & Umgiesser, G. (2014). Toward homogenization of Mediterranean lagoons and their loss of hydrodiversity. *Geophysical Research Letters*, 41(16), 5935–5941. <http://doi.org/10.1002/2014GL060843>
- Gaberšek, S., Sorgente, R., Natale, S., Ribotti, A., Olita, A., Astraldi, M. & Borghini, M. (2007). The Sicily Channel Regional Model forecasting system: initial boundary conditions sensitivity and case study evaluation, *Ocean Sci.*, 3, 31-41.
- 30
- Kantha, L.H., 1995. Barotropic tides in the global oceans from a nonlinear tidal model assimilating altimetric tides 1. Model description and results. *J. Geophys. Res.*100 (C12), 25, pp. 283–295, 309.
- Kantha, L.H. & Clayton, C.A., (2000). Numerical models of oceans and oceanic processes. *Int. Geophys.*, 66



- Krivosheya V.G., 1983. Water circulation and structure in the Tyrrhenian Sea, *Oceanology, Engl. Transl.*, 23(2), 166–171
- Hopkins, T. S., Salusti, E., & Settini, D. (1984). Tidal forcing of the water mass interface in the Strait of Messina. *Journal of Geophysical Research: Oceans*, 89(C2), 2013–2024. <http://doi.org/10.1029/JC089iC02p02013>
- 5 Luca, G., Borzelli, E., Malanotte-rizzoli, P., Gac, M., & Lionello, P. (2014). The Mediterranean Sea: Temporal Variability and Spatial Patterns, *Geophysical Monograph* 202. <http://doi.org/10.1002/9781118847572>
- Mannarini, G., Turrisi, G., D'Anca, A., Scalas, M., Pinardi, N., Coppini, G., Palermo, F., Carluccio, I., Scuro, M., Creti, S., Lecci, R., Nassisi, P., and Tedesco, L.: VISIR: Technological infrastructure of an operational service for safe and efficient navigation in the Mediterranean Sea, *Nat. Hazards Earth Syst. Sci. Discuss.*, doi:10.5194/nhess-2016-32, in review, 2016.
- 10 Marras, S., Cucco, A., Antognarelli, F., Azzurro, E., Milazzo, M., Bariche, M., ... Quattrocchi, G. (2015). Predicting future thermal habitat suitability of competing native and invasive fish species: from metabolic scope to oceanographic modelling. *Conservation Physiology*, 3(1), cou059.
- Massi, M., Salusti, E. & Stocchino, C., 1979. On the current of the Strait of Messina. *Nuovo Cimento*, 2, 543-548.
- 15 Melaku Canu, D., Solidoro, C., Bandelj, V., Quattrocchi, G., Sorgente, R., Olita, A., ... Cucco, A. (2015). Assessment of oil slick hazard and risk at vulnerable coastal sites. *Marine Pollution Bulletin*, 94(1), 84–95. <http://doi.org/10.1016/j.marpolbul.2015.03.006>
- Millot, C. (1999). Circulation in the Western Mediterranean Sea. *Journal of Marine Systems*, 20(1-4), 423–442. [http://doi.org/10.1016/S0924-7963\(98\)00078-5](http://doi.org/10.1016/S0924-7963(98)00078-5)
- Mosetti, F., (1988). Some news on the currents in the Strait of Messina. *Boll. Oceanol. Teor. Appl.*, 6, 119-201
- 20 Oddo, P., Adani, M., Pinardi, N., Fratianni, C., Tonani, M., & Pettenuzzo, D. (2009). A Nested Atlantic-Mediterranean Sea General Circulation Model for Operational Forecasting. *Ocean Science*, 5, 461–473.
- Olita, A., Dobricic, S., Ribotti, A., Fazioli, L., Cucco, A., Dufau, C., and Sorgente, R. 2012. Impact of SLA assimilation in the Sicily Channel Regional Model: model skills and mesoscale features, *Ocean Sci.*, 8, 485-496, doi:10.5194/os-8-485-2012.
- 25 Pinardi, N., & Coppini, G. (2010). Operational oceanography in the Mediterranean Sea: the second stage of development. *Ocean Science*, 6, 263–267.
- Quattrocchi, G., Cucco, A., Antognarelli, F., Satta, A., Maicu, F., Ferrarin, C., & Umgiesser, G. (2016). Optimal design of a lagrangian observing system for hydrodynamic surveys. *Journal of Operational Oceanography*. <http://doi.org/10.1080/1755876X.2015.1114805>
- 30 Sannino, G., Carillo, A., Pisacane, G., & Naranjo, C. (2015). On the relevance of tidal forcing in modelling the Mediterranean thermohaline circulation. *Progress in Oceanography*. <http://doi.org/10.1016/j.pocean.2015.03.002>
- Simeone, S., De Falco, G., Quattrocchi, G., & Cucco, A. (2014). Morphological changes of a Mediterranean beach over one year (San Giovanni Sinis, western Mediterranean). *JOURNAL OF COASTAL RESEARCH*, 217–222.



- Smagorinsky, J., (1963). General circulation experiments with the primitive equations. *Mon. Wea. Rev.*, **91**, 99–164.
- Sorgente, R., Olita, A., Oddo, P., Fazioli, L., & Ribotti, A. (2011). Numerical simulation and decomposition of kinetic energy in the Central Mediterranean: insight on mesoscale circulation and energy conversion. *Ocean Science*, *7*, 503–519.
- 5 Tonani, M., Pinardi, N., Dobricic, S., Pujol, I., & Fratianni, C. (2008). A High Resolution Free Surface Model on the Mediterranean Sea. *Ocean Science*, *4*, 1–14.
- Tonani, M., Balsamed, M., Bertino, L., Blockley, E., Brassington, G., Davidson, F., ... Wang, H. (2015). Status and future of global and regional ocean prediction systems. *Journal of Oceanography*.
- Umgiesser, G., Canu, D. M., Cucco, A., & Solidoro, C. (2004). A finite element model for the Venice Lagoon. Development, set up, calibration and validation. *Journal of Marine Systems*, *51*(1-4), 123–145.
10 <http://doi.org/10.1016/j.jmarsys.2004.05.009>
- Umgiesser, G., Ferrarin, C., Cucco, A., De Pascalis, F., Bellafiore, D., Ghezzi, M., & Bajo, M. (2014). Comparative hydrodynamics of 10 Mediterranean lagoons by means of numerical modeling. *Journal of Geophysical Research: Oceans*, *119*(4), 2212–2226. <http://doi.org/10.1002/2013JC009512>
- 15 Vercelli, F., (1925). Crociere per lo studio dei fenomeni dello Stretto di Messina. Il regime delle correnti e delle maree nello Stretto di Messina. *Comm. Intern. del Mediterraneo, Venezia*, 1-209.
- Vercelli, F., (1926). Crociere per lo studio dei fenomeni dello Stretto di Messina. *Comm. Intern. del Mediterraneo, Venezia*, 1-161.
- 20 Vetrano, A., E. Napolitano, R. Iacono, K. Schroeder, and G. P. Gasparini, 2010. Tyrrhenian Sea circulation and water mass fluxes in spring 2004: Observations and model results, *J. Geophys. Res.*, *115*, C06023.